MODIS-T Science Calibration/Characterization Plan

edited by MCST
(MODIS Characterization Support Team)

John Barker (925.0)
Peter Abel (920.1)
Bill Barnes (925.0)
Ken Brown (925.0)
Bill Eichhorn (717.3)
Wayne Esaias (671.0)
Bruce Guenther (973.0)
Forrest Hall (924.0)
Joann Hamden (925.0)
Sam Hetherington (717.3)
Yoram Kaufman (613.0)
Michael King (913.0)
Brian Markham (923)
Harvey Ostrow (925.0)
Steve Unger (923.0)
NASA Goddard Space Flight Center
Greenbelt, MD 20771

Vern Vanderbilt
Ames Research Center
Moffett Field, CA 94035

Phil Ardanuy
Harold Geller
Doug Hoyt
Shelley Petroy
Research and Data Systems Corporation
Greenbelt, MD 20770

Otis Brown
Bob Evans
Howard Gordon
University of Miami
Miami, FL 33149

Hugh Kieffer
U. S. Geological Survey
Flagstaff, AZ

Alfredo Huete
Phil Slater
University of Arizona
Tucson, AZ 85721

MODIS Science Team Meeting, Oct. 1 - 3, 1991. Attachment NN

TABLE OF CONTENTS

1 Introduction

1.1 Overview

This document is intended to provide a complete and thorough presentation of the pre-launch and in-orbit radiometric, geometric, and spectral calibration/characterization efforts designed for the MODIS-T instrument. As such, this document describes the individual efforts of the Engineering team (Code 700), specific science team members (listed on title page), and the MCST to calibrate and characterize the instrument.

1.1.1 Audience

(1) MODIS Science Management
(2) MODIS Science Team
(3) EOS Project Management
(4) EOS Project Science Office
(5) EOS Calibration Advisory Panel

1.1.2 Scope

Chapter 1 discusses the purpose and outline of this document. It includes (1) a brief description of the MODIS-T instrument and provides an overview of the science goals and how the MSCT calibration/characterization objectives fit into these goals; (2) defines the various organizations and personnel associated with the MODIS-T calibration effort and their responsibilities and interrelationships; and (3) provides schedules for the variety of prelaunch and in-orbit activities associated with the calibration/characterization effort.

Chapter 2 describes the pre-launch radiometric, spectral, and geometric calibration and characterization of the MODIS-T instrument. This section summarizes the Calibration Plan provided by the Engineering team (Code 700).

Chapter 3 provides a listing of different in-orbit radiometric calibration methods for converting on-board DN to either radiance or reflectance. It includes the background, description, justification, and algorithm development of the instrument based methods (internal sources, external solar, and external lunar), the instrument cross-comparison methods (cross se. or/within platform, cross-platform in orbit, and target related/aircraft), the target-based methods (target related/ground reflectance and bio-optical oceans), and the image related methods (radiometric rectification and class-specific scene equalization).

Chapter 4 describes the in-orbit geometric calibration effort(s).

Chapter 5 describes the in-orbit spectral calibration effort(s).

Chapter 6 provides the description of the official MODSI-T/MCST calibration algorithm.

Chapter 7 includes the data dictionary/glossary, the list of acronyms used throughout this document, and additional references.

1.1.3 Applicable Documents

(1) Earth Observing System (EOS) Project Calibration Plan, 29 July 1989, GSFC 420-0 3-01;

(2) Earth Observing System (EOS) Project Configuration Management Plan, GSFC 420-02-02;
(3) MCST Interface Control Document;
(4) MODIS-T Calibration Plan;
(5) MODIS-T Verification Plan;
(6) MODIS-T Calibration Data Book;
(7) MODIS-T Calibration Handbook.

1.2 Calibration/Characterization Objectives

1.2.1 Overview of Instrument Design

MODIS-T is a single pass grating type reflecting Schmidt imaging spectrometer. It is designed to view the Earth with a nadir footprint of 1.1 km in 32 wavelength channels of 13 to 14.5 nm from 400 to 800 nm. An interline CCD detector is used, which signal is converted to a 12 bit signal. A thirteenth bit indicates for each pixel the gain used which is different for ocean and land surfaces. This method of operation is called the dual composite mode.

Optically the instrument has a 34 mm entrance aperture and is an f/3.0 system. The CCD detector is curved in one direction to reduce spatial distortion. All metal components are aluminum except the beryllium scan mirror.

Mechanically there are four moving mechanisms. The scan, which covers 45 degrees is controlled by a continuously rotating single speed double sided mirror. The scan mirror rotates at 6.6 rpm, so each Earth scan takes 4.54 seconds. The tilt mirror rotates the scan mirror assembly about the center of the scan mirror. This direct drive mechanism allows tilts up to 55 degrees for and aft to be made. A diffuser plate is deployable on an arm and is visible to the detector when the platform is crossing the equator provided the tilt angle is less than 30 degrees. The fourth and final mechanism is an aperture wheel with 3 open aperture settings and a closed aperture which is used with a solar integrating sphere to control its radiance level.

1.2.2 Single Official Calibration Algorithm

It is the intent of the MCST, together with the MODIS-T science team, to select a single calibration algorithm which will be used as the official calibration algorithm for producing Level-1B products (radiance images). This algorithm may be selected from the methods described in Chapter 3 or it may be a combination of several of these methods. It should be stressed that this algorithm may change with time as understanding of the instrument, data characterization, and calibration methods improve.

1.2.3 Multiple Parallel Approaches

In order to have confidence that a required uncertainty has been met, several independent methods shall be used in parallel. In addition to the pre-launch calibrations and characterizations, there will be in-orbit (on-board) calibrations using lunar images, as well as in-orbit ground truth calibrations using reflectance and radiance based methods (both on-ground and aircraft). The primary purpose of these multiple pathways is to obtain, through independent means, a "calibration table" which can be used to convert instrument DN's to radiance on a routine basis (the MODIS-T/MCST calibration algorithm).

1.2.4 Comprehensive Documentation Trail

The MODIS-T calibration team (Code 700) will provide system level calibrations (radiometric, geometric, and spectral) which are traceable through documentations of data, procedures, and data analysis techniques, and the MODIS-T calibration team (Code 700) will radiometrically calibrate to a set of physical units as expressed in the Systeme International (SI) set of units. In addition, the MODIS-T calibration team (Code 700) will adhere to a common set of calibration terminologies, as sanctioned by the EOS Calibration Advisory Panel. These will be supplemented, as needed, for clarification or instrument-specific procedures.

1.3 Organizations and Responsibilities

1.3.1 EOS Calibration Advisory Panel/Calibration Office

At present, the primary responsibilities of this group include:

(1) Coordinate EOS calibration efforts;
(2) Set EOS calibration guidelines.

1.3.2 MODIS Calibration Peer Review Team

At present, the primary responsibilities of this group include:

(1) Peer review of MODIS-T characterization efforts;
(2) Develop calibration/characterization software.

1.3.3 MST Members

At present, the primary responsibilities of this group include:

(1) Set calibration/characterization requirements;
(2) Peer review of MODIS-T characterization efforts;
(3) Provide simulated MODIS-T counts data set;
(4) Conduct ground-truth calibration observations.

1.3.4 MODIS Characterization Support Team (MCST)

At present, the primary responsibilities of this group include:

(1) Coordinate MODIS-T characterization efforts
    a. Pre-Launch Radiometric
    b. Pre-Launch Spectral
    c. Pre-Launch Geometric
    d. Thermal-Infrared;
(2) Develop and deliver Level-1B calibration software;
(3) Develop and deliver Level-1B utility software;
(4) Review other satellite calibration efforts.

1.3.5 MODIS Science Data Support Team (SDST)

At present, the primary responsibilities of this group include:

(1) Integrate MCST Level-1B calibration software;
(2) Integrate MCST Level-1B utility software.

1.3.6 Earth Science Directorate (Code 900) Members

At present, the primary responsibilities of this group include:

(1) Peer review of MODIS-T characterization efforts;
(2) Provide discipline oriented expertise;
(3) Support aircraft radiance observations.

1.3.7 Engineering Directorate (Code 700)
At present, the primary responsibilities of this group include:
(1) Component testing and characterization;
(2) System level calibration/characterization;
(3) Develop software model of instrument.

1.3.8 GE Platform Integration and Test Personnel
At present, the primary responsibilities of this group include:
(1) System level tests after platform integration;
(2) Cross-calibration of instruments on platform.

1.4 Schedules
1.4.1 Overview of the Schedule
1.4.2 Software Development and Delivery to SDST
1.4.2.1 Level-1B Version 1 (Input Aircraft Data)
1.4.2.2 Level-1B Version 2 (Input Simulated MODIS Data)
1.4.2.3 Level-1B Version 3 (Integration within PGS)
1.4.2.4 Level-1B Version 4 (First In-Orbit Modifications)

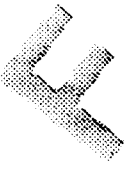

1.4.2.5 Mathematical Model Development

The MCST will develop and maintain a mathematical model of the instrument to allow performance prediction, uncertainty modeling, environmental sensitivity studies, and degradation and failure analyses. The characterization of the MODIS-T subcomponents will be of sufficient accuracy to allow meaningful analyses to be performed with this model, thus this guideline defines the subcomponent calibration specifications. Reports will be produced to document analyses and the impact of the code on instrument characterization.

1.4.3 Hardware Development and Characterization
1.4.3.1 Introduction - Multiple Instrument Characterization
1.4.3.2 Component Characterization
1.4.3.3 Subsystem Level Calibration/Characterization
1.4.3.4 System Level Calibration/Characterization
1.4.3.5 Platform Integration and Testing

2 Pre-Launch Calibration/Characterization

2.1 Objectives/Rationale
2.2 Radiometric Calibration

2.2.1 Absolute calibration

Introduction

The radiometric calibration of MODIS-T presents many challenges to the scientific and engineering community which are not easily overcome. The requirements for this calibration are quite ambitious and represent goals which are at or beyond the current state-of-the-art in the area of space orbit radiometry. The calibration of the instrument must consider not only absolute radiometric measurement against known and traceable NIST standards but also the optical characterization and testing of the complete sensor and all subsystems in any area which could affect the validity and stability of the calibration. Such areas include but are not limited to: polarization sensitivity, geometric distortion,

aberrations, flux linearity, thermal sensitivity, baffling, stray light and detector characteristics.

Approach

The basic approach for the calibration of this instrument is to characterize components, subsystems, and the full-up system at all levels of assembly. The validity of the radiometric calibration of MODIS-T requires a thorough test and characterization program in many areas including polarization and scattered light. The complete instrument will undergo absolute radiometric calibration on the ground using systems which will provide traceability to NIST standards. An on-orbit calibration system which includes the entire optical path will then be employed to verify and trace the stability of this calibration during the instrument lifetime. The on-orbit system will also monitor changes in various portions of the instrument system as well as provide for cross-calibration of the sensor with other instruments. The end result of this approach is to provide NIST traceability to each parameter used in the determination of the appropriate calibration parameters.

2.2.2 Relative calibration
2.2.2.1 Objectives/rationale

2.2.2.2 Post platform integration

MODIS-T shall be inter-compared after integration with all other optical instruments operating in the same spectral regions (e.g. ASTER, MISR, AIRS, and also with HIRIS for the C platform) using a single source. This source shall be designed to adequately fill the full aperture and cover the full field of all appropriate EOS instruments. Similarly, a single source shall be used for spectral calibration of all instruments with similar wavelength coverage.

2.3 Geometric Calibration
2.4 Spectral Calibration

3 In-Orbit Radiometric Calibration/Characterization

3.1 Objectives/Rationale

The objectives in the immediate post-launch phase will be specifically the radiometric calibration of MODIS-T, e.g. production of detector gain and offsets, determination of noise equivalent radiance, characterization of spectral sampling properties, wavelength calibration, and all other instrument parameters, accessible to evaluation using the ground-target or airborne methodologies. These characteristics will be monitored periodically throughout the instrument lifetime to provide up-to-date calibration data. Redundant calibration methods, e.g. reflectance and radiance-based determinations of gain factors, will be secured for comparison with on-board calibration data. These cumulative in-orbit determinations will constitute an instrument calibration based on Earth-directed external observations.

3.2 Instrument Based Calibration Methods

3.2.1 Internal Calibration System (ICS)

Bill Eichorn, Code 717,
GSFC, MD 20771

The MODIS-T ICS is diagrammed in Figure 3.2.1.1. It consists of an aperture mechanism containing a solar filter, a large open aperture, a small open aperture and a closed position. The aperture mechanism is in front of a large integrating sphere which collects radiation from the sun and transfers this radiation through a concentric elliptical concentrator (CEC) to a transmission diffuser which is viewable by the MODIS-T optical system once during each scan. The purpose of this section is to develop the equations used to estimate the brightness of this diffuser on orbit. The calibration system will normally be used with the solar filter in front of the integrating sphere to protect the sphere coating from degradation.

Assumptions

For the purpose of these calculations, assume that the solar spectrum can be approximated by a blackbody at 5900 K which produces an irradiance above the earth of .2 $W/m^2/Å$ or 200 $mw/cm^2/\mu m$ at 483 nm (From Handbook of Optics 3-65).

Let us assume the following nomenclature:

I_s = Solar Irradiance (200 $mw/cm^2/\mu$)

α = Angle Between the Integrating Sphere Aperture and the Sun (varies 22.5 ± 10°)

ρ_o = Reflectivity of the first portion of the integrating sphere (.98)

ρ_1 = Reflectivity of the remaining portion of the integrating sphere (.98)

A_{en} = Area of the Sphere Entrance Aperture

R_{ex} = Radius of the Sphere Exit Aperture

A_{ex} = Area of the Sphere Exit Aperture

A_d= Area of the Si Photodetector Apertures

A_o = Area of the integrating Sphere with reflectivity ρo

A_s = Internal Surface area of the integrating Sphere

F_j = Fractional Area of the jth portion of the sphere = A_j/A_S where j can = en, ex, d, or o

T_s = Transmission of the Solar Filter

R_1 = Radius of the CEC Small Aperture

A_1 = Area of the CEC Small Aperture

R_3 = Radius of the CEC Large Aperture

P_1 = Radius of the CEC remote Pupil

A_p = Area of the Remote Pupil

L = Length of the CEC

S = Separation of the CEC Large aperture and its remote pupil

ρ_c = Reflectivity of the CEC

T_i = Transmission of the ICS Diffuser

A_i = Area of the ICS Diffuser

β_o = Angle between the transmission diffuser normal and the axis of the CEC at tilt = 0

β = Angle between the transmission diffuser normal and the axis of the CEC at tilt = τ

ρ_f= Reflectivity of the periscope fold flat

ρ_m = Reflectivity of CEC coupling Flat

T_c = Transmission of the CEC-Sphere coupling

MODIS-T Optical System Sees
25 Frames of ICS Diffuser data during
each 180° of scan mirror rotation. The
ICS Diffuser always fills the optical system FOV

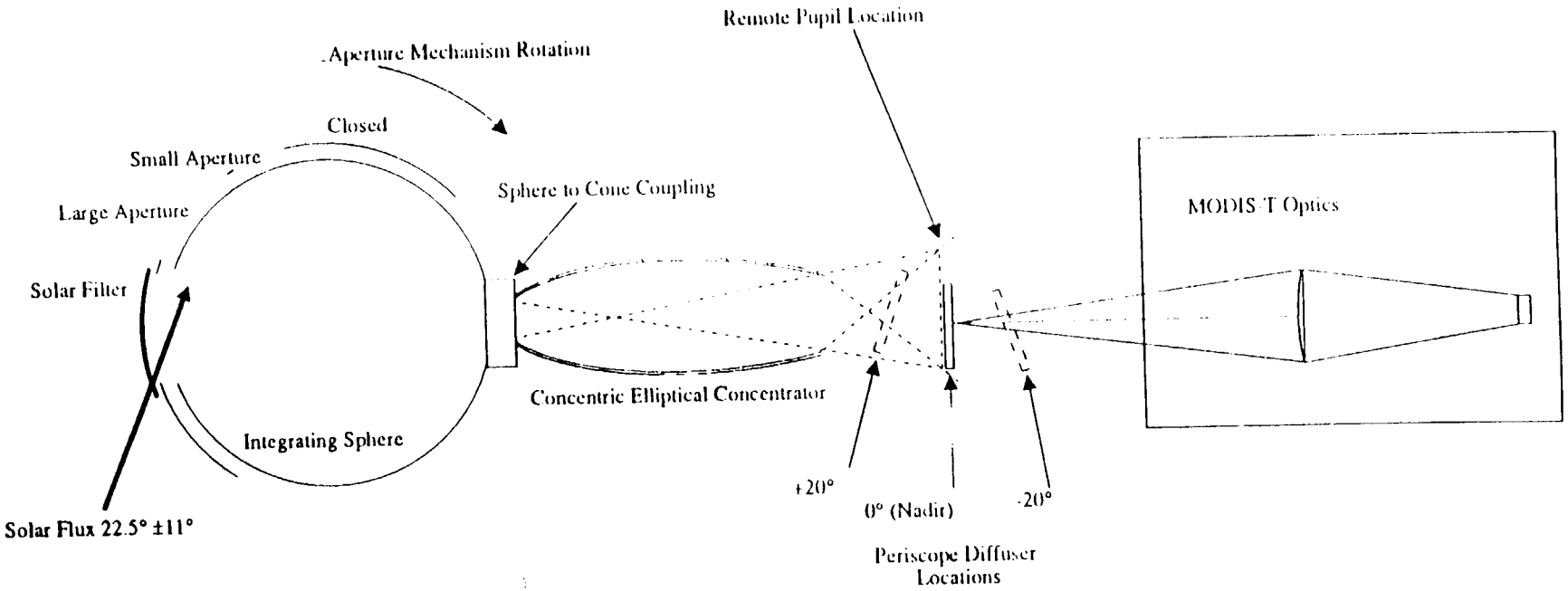

MODIS-T Internal Calibration System Concept

B_{ICS} = Apparent brightness of the ICS
L_d = ICS diffuser location with respect to CEC remote pupil. (Ld = 0 then diffuser is at pupil)

Formulas

The flux entering the integrating sphere, F_{in}, is given by

$$F_{in} = I_S T_S A_{en} \sin(\alpha) \quad (1)$$

Let us assume that the integrating sphere has essentially two reflectivities (ρ_o and ρ_1) where ρ_o is the reflectivity of the portion of the sphere which is directly illuminated by solar radiation (and may degrade with time) and ρ_1 is the reflectivity of the sphere which is diffusely illuminated by the radiation in the cavity. Initially, these reflectivities are equal. The fractional area of the sphere which has reflectivity ρ_o is assumed to be F_o (=.3). The reflectivities of the four detector ports and the exit aperture are assumed to be 0. In this case, the through-put of the integrating sphere, Q_s, is given by

$$Q_s = \frac{\rho_o F_{ex}}{[1 - \rho_1 (1 - F_{en} - F_{ex} - 4F_d - F_o) - \rho_o F_o]} \quad (2)$$

The flux at the exit port of the integrating sphere is then given by

$$F_{in} * Q_s$$

The integrating sphere is connected to the CEC by some yet TBD method. Packaging constraints seem to preclude the CEC being attached directly to the sphere. Some loss of flux must be assumed at this juncture to allow for this packaging. Let us assume that the CEC is separated from the sphere by some distance, X_c, and that a fold mirror with reflectivity ρ_m is used to couple the sphere output to the CEC. If the CEC were directly connected to the sphere, all the flux at the sphere output port would enter the CEC and be transmitted to the CEC's remote pupil. As the CEC is moved a distance Xc away from the sphere, the flux which enters the CEC is reduced by the factor T_c where

$$T_c = 1 - \frac{1}{[1 + \left(\frac{R_{ex}^2}{X_c}\right)]} \quad (3)$$

Hence the flux entering the CEC, F_c, is given by

$$F_c = F_{in} Q_s \rho_m T_c \quad (4)$$

This is also the flux which passes through the CEC remote pupil by virtue of the properties of the CEC. If one assumes that the flux is uniformly distributed at this location, then the flux density at the CEC remote pupil location is given by

$$\frac{F_c}{A_p} \tag{5}$$

If the ICS transmission diffuser is located at this remote pupil, then the flux intercepted by the diffuser is given by

$$\frac{A_i \cos(\beta)\, F_c}{A_p} \tag{6}$$

Some assumption needs to be made about how the transmission diffuser scatters the light. Let us assume the diffuser is lambertian. This is probably not a good assumption but it is expected to underestimate the the brightness of the diffuser since most of the radiation will be forward-scattered. With this assumption, the diffuser brightness as seen through the periscope fold flat is given by

$$B_{ICS} = F_c\left(\frac{A_i \cos(\beta)}{A_p}\right)\left(\frac{\rho_f}{\pi}\right) \tag{7}$$

Let us now become a bit more general. As the periscope tilts, the diffuser location changes. It is not in general located at the CEC remote pupil. For the purposes of this estimation, let us assume that the flux from the CEC leaves the CEC in a cone which has an angle given by the limiting ray angle of the CEC. This angle, ψ, is given by the equation

$$\tan(\psi) = \frac{R_3 - P_1}{S} \tag{8}$$

The assumption which we are making now is that the flux after the CEC large aperture, F_c, is uniformly distributed into a cone with the above angle. If this is the case, the flux density varies as the position of the diffuser moves. If the location of the diffuser with respect to the remote pupil is given by L_d, then the radius of the cone with uniform flux density at the diffuser location is given by

$$R = R_3 + \tan(\psi)\, L_d \tag{9}$$

and the flux density at this location is given by

$$\frac{F_c}{\pi R^2} = \frac{F_c}{(\pi(R_3 + \tan(\psi)\, L_d)^2)} \qquad (10)$$

The flux intercepted by the ICS diffuser at this location is given by

$$\frac{F_c A_i \cos(\beta)}{(\pi(R_3 + \tan(\psi)\, L_d)^2)} \qquad (11$$

where β is the angle between the diffuser normal at the tilt angle τ and the CEC optical axis ($= \beta o + \tau$). The brightness of the diffuser is now given by

$$B_{ICS} = \frac{F_c\, A_i \cos(\beta_o + \tau)}{(\pi(R_3 + \tan(\psi)\, L_d)^2)} \left(\frac{\rho}{\pi}\right) \qquad (12)$$

which can be written as

$$B_{ICS} = \frac{F_{in}\, Q_s\, \rho_m\, T_c\, A_i \cos(\beta_o + \tau)}{(\pi(R_3 + \tan(\psi)\, L_d)^2)} \left(\frac{\rho}{\pi}\right) \qquad (13)$$

Calculations

A spreadsheet has been developed which calculates the ICS diffuser brightness per the above assumptions. A sample spreadsheet is attached along with a spectral radiance curve for that spreadsheet.

3.2.2 External Solar

3.2.3 External lunar

H.H. Kieffer and R.L. Wildey, U.S. Geological Survey, Flagstaff, AZ 86001

Introduction

In-flight calibration of imaging instruments is a difficult task. Calibration subsystems themselves are subject to offset and drift, and many do not calibrate the entire optical system, which can be done only by having external, full aperture sources, such as solar diffuser surfaces. Calibration can be done through the use of well characterized ground targets, but this requires near-simultaneous measurements, a substantial ground campaign, and a difficult correction for the atmosphere.

The objective of this work is to provide new radiometric information needed to allow the moon to be used as a well-characterized radiometric source for calibration of earth-orbiting instruments that can view it. In addition to direct use of the radiometric

information, such detailed knowledge of the lunar brightness enables better use of the moon for measurement of the MTF and scattered light performance of the instruments.

Background

The moon has several unique properties: it is within the dynamic range of most imaging instruments, it is surrounded by a black field in both reflective and thermal band, and its surface brightness distribution can be better known than that of any other natural object at which most instrument can be safely pointed. Although the moon's photometric properties are thought to be intrinsically constant over long time scales (natural rate of change estimated at 10^{-9} percent per year [1]), the effects due to the variation of illumination conditions and observation geometry must be considered. These in turn are related primarily to the lunar photometric function and the lunar libration

The libration of the moon, the change of the position of the sub-earth point on the moon, results from the axial inclination and the small change in the angular velocity of the moon around the earth due to eccentricity of the lunar orbit (optical libration) and small nonuniformity in the rotation rate of the moon (physical libration). These combine to yield a variation of about $\pm$ 7° in both latitude and longitude, both with a period of near one month, but with small differences that require the dual precessional cycle of 18.6 years (accidently approximately the same length as the Saros cycle) to complete.

The variations of albedo over the face of the moon are common knowledge. Quantitatively, at modest spatial resolution the normal albedo (in V band) ranges from 9% to 23%, with a mean value near 12.5% [2]. Albedo variegation extends to scales below the limit of telescopic resolution. The moon appears gray in the visible, but has a general increase in reflectivity into the near infrared [3]. Variation of color between different locations on the moon is small, and those spectral features that do exist are relatively broad [4,5].

The moon does not behave as an ideal diffuse reflector. As the phase angle (sun-moon-observer angle) becomes small, the moon brightens dramatically; this is called the "opposition effect" [6], which increases up to the point that lunar eclipse begins. Current knowledge of the lunar photometric function is limited to a few wavelengths, and to a few small areas or for the spatially-integrated lunar brightness (the phase function) [7,8].

The moon has several additional characteristics that require consideration in treating it as a radiometric standard. Light from the whole moon has small negative polarization at small phase angles, becoming most negative at ~ -1.2% near a phase angle ~ 12°, then increasing through 0 polarization near 24° up to about +8% at phase angles near 90°. Individual areas (appropriate for HIRIS spatial resolution) typically have polarization at phase angles less than 15° of 1.2% or less at 361 nm, and polarization decreases toward longer wavelengths out to at least 1 μm [9]. The degree of polarization is approximately inversely proportional to albedo, being greatest for dark areas, and least for bright areas [6]. Variations with albedo are small for phase angles less than about 40°. Early work indicated that near full moon, polarization near the limb of the moon was about 0.1-0.2% parallel to the limb [10].

Because the surface of the moon can become as hot as 400 K[11], thermal emission becomes important for longer wavelengths. Thermal emission at 400 K contributes about 0.1% at 1.8 μm, 1% at 2.0 μm, and 10% at 2.3 μm. Thermal models and prior infrared measurements [12] would allow correction for thermal emission to about 1/5 of these

levels. Simultaneous measurements of lunar radiance near 3.5 μm would allow correction for thermal emission to better than 0.5%.

Approach

Current knowledge of the radiometry of the moon is limited to attempts to calibrate the absolute spectral reflectance at a few points [13], and measurements of the integrated lunar brightness at a few wavelengths [7]. In order to support the spatial resolution of EOS instruments, especially HIRIS, extensive radiometric observations will be made with spatial (angular) resolution of 4.4 arcsec, twice as fine as HIRIS. The wavelengths of reasonable transparency of the earths' atmosphere between 0.3 and 2.5 μm will be covered. Because the technology to do radiometry with imaging spectrometers has not yet been developed, radiometry will be at a discrete set of passbands by use of interference filters; on the order of 20 wavelengths will be used.

Two filter imagery systems will operate simultaneously, one in the VIS and one in the VNIR. Each will have its own telescope, boresighted and supported on a common mount. No beam splitter or fold mirrors will be involved and each telescope and detector system will be axial, so that the detection systems should be polarization-insensitive.

For wavelengths from 0.3 to 1.0 μm, a conventional astronomical silicon CCD will be used, with 512 x 512 pixels. No "off-the-shelf" photometric arrays are available for wavelengths longer that 1 μm, and this project had planned to use an array produced as part of the HIRIS development. The exact type of infrared array to be used is still under study, but it is assumed that a 256-square array with characteristics similar to HIRIS test arrays will be available.

An in-dome radiometric standard will be observed at least as often as the beginning and end of astronomical observations each night. This standard will utilize a NIST-traceable halogen standard lamp and a nearly ideal diffusing surface large enough to illuminate the full aperture of the telescopes. Our plan is that this facility be part of the circuit for the EOS portable radiometer standard (Phil Slater proposal), and the connection to NIST be established every 6 months.

The telescope system will be highly automated and entirely under computer control. Most of the telescope time will be spent observing standard stars, especially those in a band along the moons' orbit. This both allows quantitative determination of atmospheric extinction (needed to correct to exo-atmospheric radiances) and ties the radiometric system to the existing standard star system. Experiments "trailing" stars at different rates will be done to determine the best radiometric techniques and to determine the high-frequency variation of apparent radiance due to atmospheric lensing (scintillation).

Design and planning for this lunar radiometry facility has begun, and routine observations are scheduled to begin in the fall of 1993. Observations would continue at least 4 1/2 years; observations over at least 1/4 the Saros cycle are required to cover the range of lunar libration.

Observations will be made each month when the moon is at 90° phase or less (the bright two weeks of each lunation) on all photometric nights (at the planned observatory site in Flagstaff, there are approximately 100 photometric nights each year). In order to develop a photometric model for each resolution element on the moon, all observations will be reduced to a special projection that incorporates all areas of the moon visible from the

earth over the full range of libration, yet has minimum distortion from the appearance of the moon for a single observation. Observations will be reduced to produce a photometric model of each pixel in this projection for each wavelength band.

Initial error budget analysis that the expected long-term precision is ~0.8%, and absolute radiance ~2.3%. The largest contribution to uncertainty of absolute radiometric accuracy is the calibration of the standard lamp.

For the nominal EOS platform orbit, the average angular size of the moon is equivalent to a nadir target of 6.73 km. Instruments of 15 m , 30 m, 250 m, and 1 km resolution would have 425, 212, 25.5 and 6.4 pixels across the moon, respectively.

Because the moon is darker than most terrestrial scenes, spacecraft calibration observations of the moon should be made at small phase angles if possible to avoid being low in the dynamic range of the instrument. Spacecraft observations could be made at any phase angle greater than 1.5°, where lunar eclipse phenomena begin. The moon attains a minimum phase angle of less than about 6° each month, and near zero twice a year.

Expected Results

For any specific spacecraft observation, the precise illumination and observation geometry will be used to calculate a radiometric image of the moon at full model spatial resolution in each wavelength. This radiometric image will then be geometrically transformed to match the resolution and orientation of the spacecraft instrument image. (The spatial uncertainty in resampling to a specific HIRIS observation increases the overall radiometric uncertainty 0.1%, other instruments would be similar for pixels that are fully on the moon). The team for that instrument would produce a radiometric image based on their calibration files. The ratio of the two images represents the factor between the two calibration systems.

Such radiometric images can also be used in reduction of instrumental scans across the moon for study of MTF and scattered light sensitivity [1], although for these purposes the spatial resolution and radiometric precision of this study would rarely be needed.

Preliminary calculations of lunar radiance levels, with about 15% uncertainty, are now available for use in design of instrument gain settings.

References

[1] Kieffer, H.H. and R.L. Wildey, 1985. Absolute calibration of Landsat instruments using the Moon; *Photogram. Eng. and Remote Sens.*, 51, 1391-1393.

[2] Wildey, R.L., 1976. A digital file of lunar normal albedo. *The Moon*, 16, 231-277.

[3] McCord, T.B. and T.V. Johnson, 1970. Lunar spectral reflectivity (0.30 to 2.50 microns) and implications for remote mineralogical analysis. *Science*, 169, 855-858.

[4] McCord, T.B., M.P. Charette, T.V. Johnson, L.A. Lebofsky, C. Pieters, and J.B. Adams, 1972. Lunar spectral types. *J. Geophys. Res.*, 77, 1349-1359.

[5] Pieters, C.M. and J.F. Mustard, 1988. Exploration of the crustal/mantle material for the Earth and Moon using reflectance spectroscopy. *Remote Sens. of Environ.*, 24, 151-178.

[6] Gehrels, T., T. Coffeen, and D. Owings, 1964. Wavelength dependance of polarization. *III. The Lunar Surface. Astron. Jour.*, 69, 826-852.

[7] Lane, A.P. and W.M. Irvine, 1973. Monochromatic phase curves and albedos for the lunar disk. *Astron. Jour.*, 78, 267-277.

[8] Helfenstein, P. and J. Veverka, 1987. Photometric properties of lunar terrain derived from Hapke's equation. *Icarus*, 72, 342-357.
[9] Dollfus, A., 1961. Polarization studies of the planets, in Planets and Satellites, G.P. Kuiper and B.M. Middlehurst, eds., 343-399.
[10] Lyot, B., 1929. Annuals Observatoire Meudon, vol. 8, part 1.
[11] Shorthill, R.W., 1972. The infrared moon: a review. In Thermal Characteristics of the Moon, J.W. Lucas, ed., *Progress in Astronautics and Aeronautics*, vol. 28, the MIT Press, 3-49.
[12] Sarri, J.M. and R.W. Shorthill, 1967. Isothermal and isophotic atlas of the moon: contours through a lunation. NASA Contractors Report CR-855, 186 pp.
[13] McCord, T.B., R.N. Clark, B.R. Hawke, L.A. McFadden, P.D. Owensby, and C.M. Pieters, 1981. Moon: near-infrared spectral reflectance, a first good look. *J. Geophys. Res., 86 (B11)*, 10, 833-10,892.

3.3 Instrument Cross-Comparison Methods

3.3.1 Cross-Sensor/Within Platform

Phil Slater et al., University of Arizona

Introduction

One method for the cross-calibration of different instruments on the same platform is identical to that used by the University of Arizona for the calibration of AVHRR with respect to TM. It should be emphasized that cross-calibration of instruments on the same platform eliminates uncertainties associated with different illumination and viewing geometries.

The University of Arizona group plans to make in-orbit calibrations of high spatial resolution EOS sensors such as ASTER (and HIRIS for the C platform) using a reflectance-based method which references a well characterized ground site such as White Sands [1]. MODIS in-orbit calibration with reference to a ground site shall be done with a method similar to its AVHRR work [2]. The reflectance-based method is discussed in more detail in Section 3.4.1

Results

The University of Arizona group has found that the responsiveness of channels 1 and 2 of the AVHRR on NOAA-9 and -10 has degraded significantly since launch [2]. The group has refined its reflectance-based method and applied the refinements to its TM calibrations [3]. The group has also developed a refinement to its reflectance-based method which uses measurements of the diffuse and total irradiance at the surface [4].

The University of Arizona group is currently analyzing channels 1 and 2 of the AVHRR on NOAA-11. Preliminary investigations show degradation of approximately 5 and 15 percent in channels 1 and 2.

The University of Arizona group plans to continue with this type of work with future AVHRR and follow-on sensors and a MODIS simulator if it becomes available. The group plans to refine its methods to include the use of a field SWIR spectrometer, a solar radiometer designed to measure total column water vapor, and an imaging solar radiometer which will be used to study the solar aureole. The aureole is a sensitive indicator of aerosol scattering and the group hopes to improve its knowledge of the scattering phase function with this future instrument.

References

[1] Slater, P.N., S.F. Biggar, R.G. Holm, R.D. Jackson, Y. Mao, M.S. Moran, J.M. Palmer, and B. Yuan, 1987. Reflectance- and radiance-based methods for the in-flight absolute calibration of multi-spectral sensors, *Rem. Sens. of Environ.*, 22, 11-37.

[2] Teillet, P.M., P.N. Slater, Y. Mao, B. Yuan, R.J. Bartell, S.F. Biggar, R.P. Santer, R.D Jackson, and M.S. Moran, 1988. Absolute radiometric calibration of the NOAA AVHRR sensors, *Proc. SPIE*, Vol. 924, Recent Advances in Sensors, Radiometry, and Data Processing for Remote Sensing, 196-207.

[3] Hart, Q.J., "Refinements to the reflectance-based absolute radiometric calibrations of the Landsat-5 Thematic Mapper," Proc. SPIE, in press (1991).

[4] Biggar, S.F., Santer, R.P., and Slater, P.N., "Irradiance-based calibration of imaging sensors," Proc. IGARRS 90 Vol. 1, pp. 507- 510 (1990).

3.3.2 Cross-Platform In-Orbit

The University of Arizona group has investigated the calibration of a low spatial resolution imaging sensor by reference to a higher resolution "calibrated" sensor [1,2]. This work has been funded under a NASA grant and is ongoing. The AVHRR sensors on the NOAA 9, 10, and 11 satellites have been calibrated with reference to the Thematic Mapper (TM) and Systeme Probatoire d'Observation de la Terre (SPOT) HRV cameras. The high resolution sensor is calibrated with reference to a ground site such as White Sands, New Mexico. This calibration is normally done using a ground reflectance-based method (see Section 3.4.1 for more details on this method). Pixels from a high resolution calibrated image (taken nearly coincident with the low resolution image) are spatially registered and then aggregated to the spatial resolution of the AVHRR image. Corrections are made for sensor spectral response differences and for the ground target bidirectional reflectance factor (BRF) if the sensor acquisition geometries are significantly different. The ground reflectance is determined from the calibrated high resolution image [3]. Spatially uniform areas on a scale of multiple low resolution pixels are used in a reflectance-based method to determine the calibration of the AVHRR sensor. The atmospheric correction is normally done using spectral optical properties measured from the ground at the target site during the high resolution image acquisition.

References

[1] Teillet, P.M., P.N. Slater, Y. Mao, B. Yuan, R.J. Bartell, S.F. Biggar, R.P. Santer, R.D Jackson, and M.S. Moran, 1988. Absolute radiometric calibration of the NOAA AVHRR sensors, *Proc. SPIE*, Vol. 924, Recent Advances in Sensors, Radiometry, and Data Processing for Remote Sensing, 196-207.

[2] Che, N., Grant, B.G., Flittner, D.E., Biggar, S.F., Slater, P.N., Jackson, R.D., and Moran, M.S., "Results of Calibrations of the NOAA-11 AVHRR made by reference to calibrated SPOT Imagery at White Sands, New Mexico, "Proc. SPIE, in press (1991).

[3] Holms, R.G., M.S. Moran, R.D. Jackson, P.N. Slater, B. Yuan, and S.F. Biggar, 1989. Surface Reflectance Factor Retrieval from Thematic Mapper Data, *Rem. Sens. of Environ.*, 27, 47-57.

3.3.3 Target related/aircraft

Peter Abel, Code 920, GSFC, Greenbelt, MD 20770

Introduction

Satellite radiometers observing the Earth in the visible and near infrared (visnir) spectrum (~400 to 1100 nm) have usually suffered significant losses in gain while in orbit. For example, Advanced Very High Resolution Radiometer (AVHRR) visnir channels have shown gain loss rates ranging from 7% per year (NOAA-9) [1] to nearly zero (NOAA-6), and CZCS results for the four years after launch indicate that degradation is more rapid at shorter wavelengths (average degradation rate of 7% per annum for Channel 1 at 443 nm, falling to less than 1% per annum for Channels 3 and 5, at 550 and 670 nm respectively [2]). A primary objective of aircraft studies is therefore to measure the absolute gain of the MODIS-T visnir channels and their rate of change in orbit. Based on results from other satellite sensors, it would be necessary to collect such measurements at least twice a year (more frequently immediately after launch) to establish the gain to the accuracy required for useful application in global change science.

MODIS-T will have an onboard radiance calibration system for the visnir channels, but the system represents technology that is unproven in space. A second objective is therefore to provide independent calibration data to validate the performance of the onboard system.

MODIS-T's instrument's scan mirror, if contaminated in space, will cause the channel gains to become dependent on scan angle. No measurements of this dependence will be available from the onboard calibration systems, so a third objective is to measure gain as a function of scan angle. The most critical measurement is expected to be for the along-track scan of MODIS-T. This should be done immediately after launch, and at least every two years thereafter.

Approach

Figure 3.3.3.1 illustrates the method, which uses a sunlit, optically stable, highly reflective and cloud-free ground target as a transfer standard between a well-calibrated spectroradiometer on the aircraft and the radiometer on the satellite. The method depends on accurate prediction of the satellite-target viewing geometry, which is necessary to enable the aircraft spectroradiometer to be coaligned with the satellite view vector during satellite overpass. Small corrections must be applied to account for the effects of the atmospheric path between the aircraft and the satellite, and to account for the difference between the footprints of the two instruments on the target. These corrections, and knowledge of the spectral response function of a given channel of the satellite radiometer, allow the calculation of equivalent sets of radiance values (from the aircraft measurements) and count values (from the satellite measurements) that correspond to the altitude of the satellite radiometer and the field-of-view of the aircraft spectroradiometer. These sets are augmented in the case of AVHRR, for example, by the measurement of the count corresponding to the radiance of space, which is assumed to be zero. A least squares fit between the sets gives the gain (i.e. count output divided by radiance input) of the satellite radiometer's channel as the slope of the best-fit line.

The atmospheric correction is minimized by operating the aircraft in the stratosphere, so the necessary corrections are limited to stratospheric aerosol and stratospheric ozone. In this case the atmospheric correction for reasonable observation geometry is calculated to be less that 3% for channel 1 of AVHRR and is smaller for channel 2. The correction may be calculated to adequate accuracy, in the absence of recent additions of aerosols of volcanic origin, by adopting climatological averages for stratospheric composition, and calculating the correction with the LOWTRAN-7 [3] computer code. The aircraft spectroradiometer collects data for a period of approximately 3 minutes over the target. Satellite data encompassing the spatial range of the aircraft data are collected from the satellite radiometer

MODIS-T Internal Calibration System Flux and S/N

Single Integrating Sphere				ICS Nominal Pixel = 0 Tilt Angle = 0.0 Sun Angle = 22.5		ICS Maximum Pixel = 1 Tilt Angle = +20.0 Sun Angle = 33.5		ICS Minimum Pixel = 1 Tilt Angle = -20.0 Sun Angle = 11.5	
Band	Wavelength (nm)	LTYPICALO mw/cm^2 /sr/μ	LTYPICALO S/N (SPEC)	Internal Calibrator (ICS) mw/cm^2/sr/μ	ICS S/N	Internal Calibrator (ICS) mw/cm^2/sr/μ	ICS S/N	Internal Calibrator (ICS) mw/cm^2/sr/μ	ICS S/N
1	410	4.59	820	0.855	153	1.737	310	0.291	52
2	425	4.38	859	0.879	172	1.785	350	0.299	59
3	440	4.20	838	0.897	179	1.820	363	0.305	61
4	455	3.91	826	0.908	192	1.844	390	0.309	65
5	470	3.64	814	0.915	205	1.857	415	0.311	70
6	485	3.36	802	0.916	219	1.860	444	0.312	74
7	500	3.09	786	0.914	232	1.855	472	0.311	79
8	515	2.91	770	0.908	240	1.842	488	0.309	82
9	530	2.67	754	0.898	254	1.823	515	0.305	86
10	545	2.43	752	0.886	274	1.799	557	0.301	93
11	560	2.10	750	0.872	311	1.770	632	0.296	106
12	575	2.00	736	0.855	315	1.737	639	0.291	107
13	590	1.90	724	0.838	319	1.701	648	0.285	109
14	605	1.81	711	0.819	322	1.662	653	0.278	109
15	620	1.70	699	0.799	328	1.622	667	0.272	112
16	635	1.61	661	0.778	320	1.580	649	0.265	109
17	650	1.49	616	0.757	313	1.537	635	0.257	106
18	665	1.37	571	0.736	307	1.494	623	0.250	104
19	680	1.31	558	0.714	304	1.450	618	0.243	103
20	695	1.25	546	0.693	303	1.406	614	0.236	103
21	710	1.19	535	0.671	302	1.363	613	0.228	103
22	725	1.12	522	0.650	303	1.320	615	0.221	103
23	740	1.05	508	0.629	304	1.277	618	0.214	103
24	755	0.99	495	0.609	304	1.236	618	0.207	103
25	770	0.93	490	0.588	310	1.195	629	0.200	105
26	785	0.88	472	0.569	305	1.155	619	0.193	104
27	800	0.83	454	0.549	301	1.115	610	0.187	102
28	815	0.78	435	0.531	296	1.077	601	0.180	101
29	830	0.73	417	0.512	293	1.040	594	0.174	100
30	845	0.68	398	0.495	290	1.004	588	0.168	98
31	860	0.63	380	0.478	288	0.970	585	0.162	98
32	875	0.58	317	0.461	252	0.936	511	0.157	86

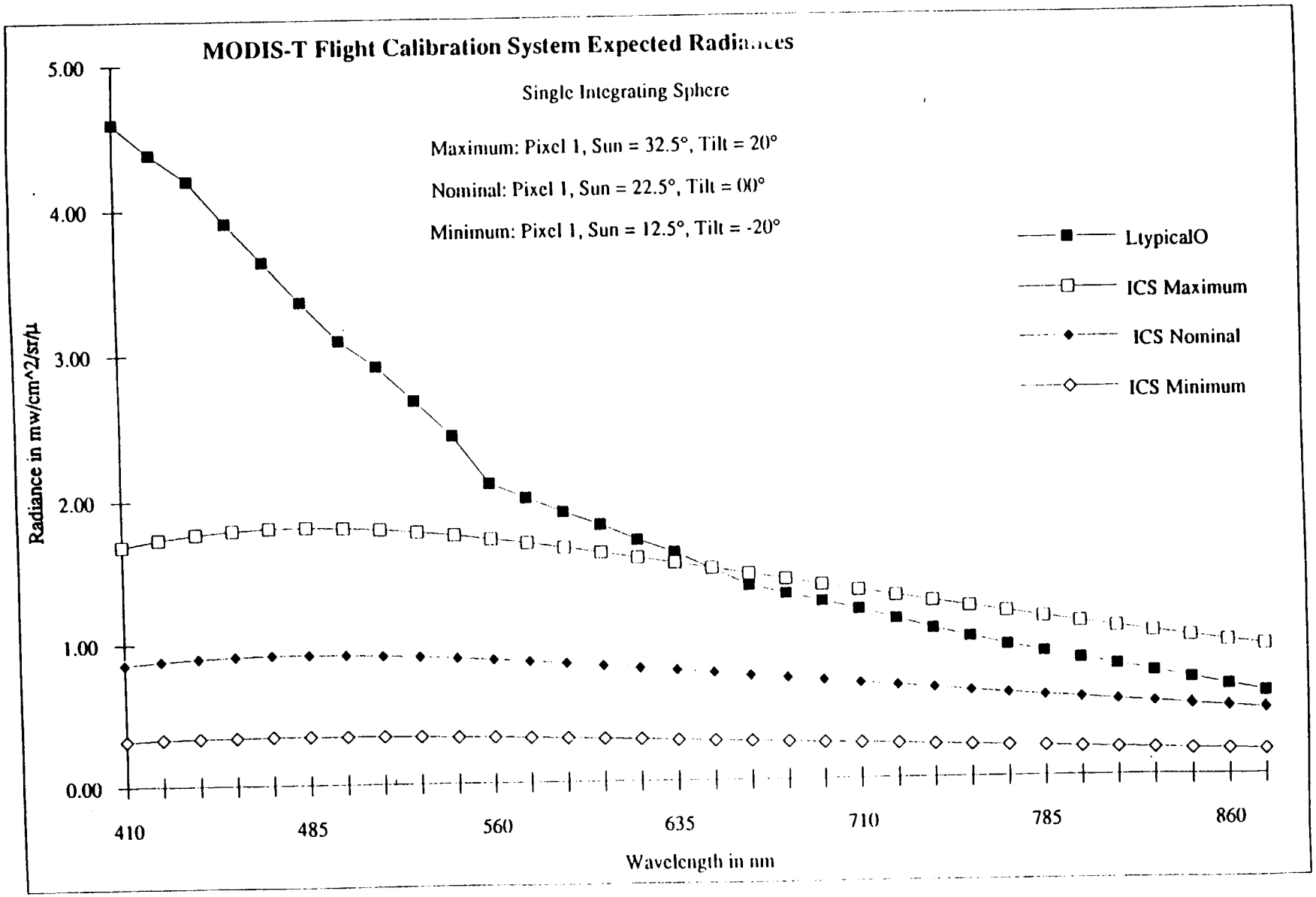
MODIS-T Flight Calibration System Expected Radiances
Single Integrating Sphere
Maximum: Pixel 1, Sun = 32.5°, Tilt = 20°
Nominal: Pixel 1, Sun = 22.5°, Tilt = 00°
Minimum: Pixel 1, Sun = 12.5°, Tilt = -20°
LtypicalO
ICS Maximum
ICS Nominal
ICS Minimum
Radiance in mw/cm^2/sr/μ
5.00
4.00
3.00
2.00
1.00
0.00
410
485
560
635
710
785
860
Wavelength in nm

Modis-T Solar Calibration System Single Integrating Sphere w/ Concentric Elliptical Concentrat				
Angle Of Incidence	deg	22.5000	0.383	3.1416
Incident Flux	mw/cm^2-μ	200.0000		0.9900
First Integrating Sphere			Area (cm^2)	
First Sphere Diameter	in	10.0000	2026.830	1.0000
Initial Area in Percent of Total			0.300	0.3000
Ent Port Diameter	in	4.0000	81.073	0.0400
Exit Port Diameter (Dex)	in	1.5000	11.401	0.0056
Detector 1	in	0.3937	0.785	0.0004
Detector 2	in	0.3937	0.785	0.0004
Detector 3	in	0.3937	0.785	0.0004
Detector 4	in	0.3937	0.785	0.0004
Initial Reflectivity (Rho0)		0.9800	SFi	0.3472
Reflectivity (Rho1)		0.9900	1-Rho*SFi-Rho0*Fo	0.0597
Effecuency at Exit Port		0.0923	Efficency	0.0933
Solar Fluer Transmission (Ts)		0.9800		
Flux In	mw/μ	6080.9724		
Flux Out of Exit Port	mw/μ	561.4662		
Flux into Si Det	mw/μ	39.0735		
Exit Port Brightness	mw/cm^2-sr-μ	15.6760		
Sphere Wall Brightness (ExRad)		15.6760		
Second Integrating Sphere (NOT USED)			Dual Sphere Flag	0
Second Sphere Diameter	in		0.0000	2.2500
Ent Port Diameter	in			2.2500
Exit Port Diameter	in		0.0000	1.5000
Det 1	in			0.3937
Det 2	in			
Line1	in			
Line2	in			
Reflectivity				0.9900
Sphere Eff at Exit Port				
Sphere Eff at Entrance Port				
Flux into Sphere	mw/μ			
Flux Out First Order	mw/μ			
Actual Flux Out (Using Trout Formula)	mw/μ			
Exit Port/Sphere Wall Brightness	mw/cm^2-sr-μ			
Concentric Elliptical Concentrator			Area (cm^2)	
Sphere Exit Port Diameter	in	1.5000	11.401	
Flux Available to CEC at Sphere Exit	mw/μ	561.4662		
Exit Port Brightness (ExRad)		15.6760		
CEC Small Aperture (SmAp) (Asmap)	in	1.5000	11.401	
CEC Length	in	11.6472		
CEC Large Aperture	in	3.2178		
Remote Pupil Diameter	in	5.0000		
Rem. Pupil Distance from Large Aperture	in	4.4000		
CEC Separation Distance (Sep)	in	0.4000		0.4000
Flat Reflectance (Rflat)	%	1.0000		
Flux into CEC (CECFlux)	mw/μ	437.1277	437.128	
CEC Coupling Coef		0.7785		
Flux Into CEC	mw/μ	437.1277		
CEC Reflectivity		0.9800	Area (cm^2)	
Flux Into Remote Pupil (RPFlux)	mw/μ	428.3851	126.677	
Remote Pupil Size (Diameter)	in	5.0000	126.677	
Remote Pupil X Location				
Remote Pupil Y Location				
Irradiance at Pupil Location	mw/cm^2-μ	3.3817		
Diffuser Screen			Area (cm^2)	
Sec Diffuser Reflectivity (Rsd)		0.9800		
Sec Diffuser Height	in	2.6680	34.081	
Sec Diffuser Width	in	1.9800		
Periscope Tilt Angle	deg	90.0000		
Sec Diffuser Angle from Horizontal	deg	0.0000		
Sec Diffuser angle re Conc Axis (Ad)		90.0000		
Sec Diffuser Center X Location RE Pupil		0.9000		
Sec Diffuser Center Y Location RE Pupil		-1.0000		
Flux Cone Height at Diffuser		5.3645	145.822	
Irradiance at Diffuser Location	mw/cm^2-μ	2.9377		
Flux Incident onto Diffuser	mw/μ	100.1219		
Secondary Diffuser Brightness	mw/cm^2-sr-μ	0.9164	0.5183	1.2867
Solar Diffuser Brightness @ 100%	mw/cm^2-sr-μ	63.6620		
Ratio		0.0144	0.0081	0.0202
Solar Diffuser Brightness @ 5%	mw/cm^2-sr-μ	3.1513	0.0094	

Figure 3.3.3.1. (A) The aircraft spectroradiometer observes the target along the same view vector as the satellite sensor. The two instruments have different footprints, and the ground tracks of aircraft and satellite may be different.

(B) The radiance for each wavelength in a scan corresponds to a different footprint. Corrections are applied in the analysis by interpolation to INS times.

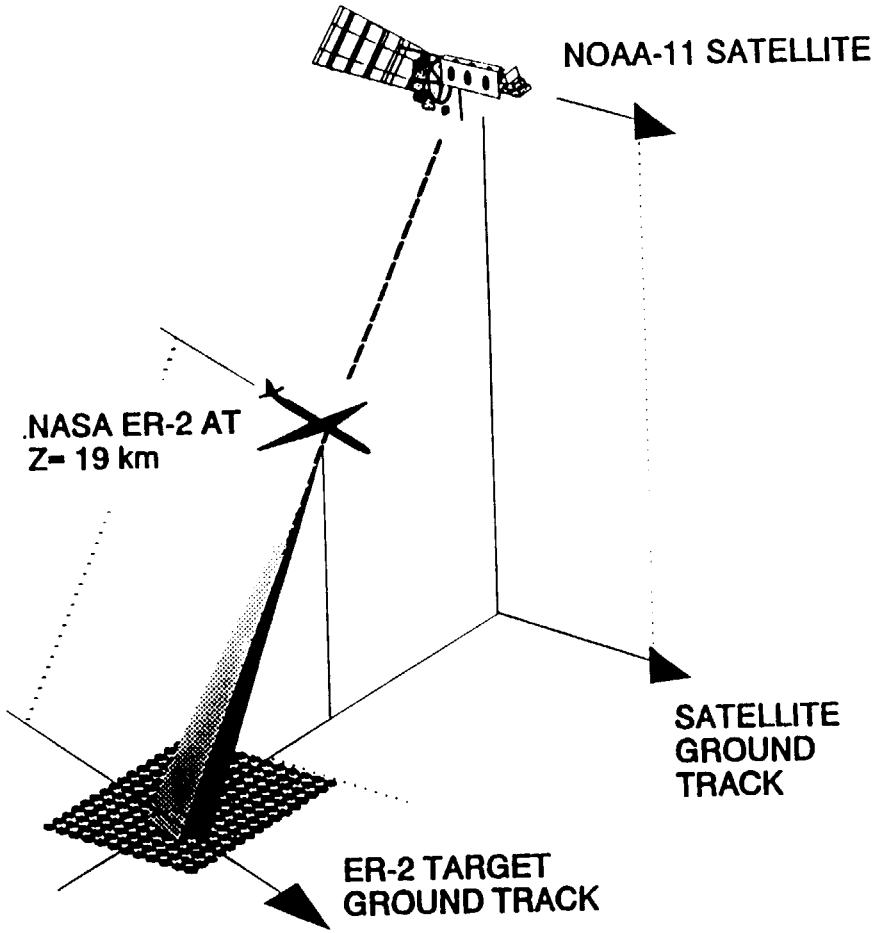

(A) CONGRUENT OBSERVATION GEOMETRY

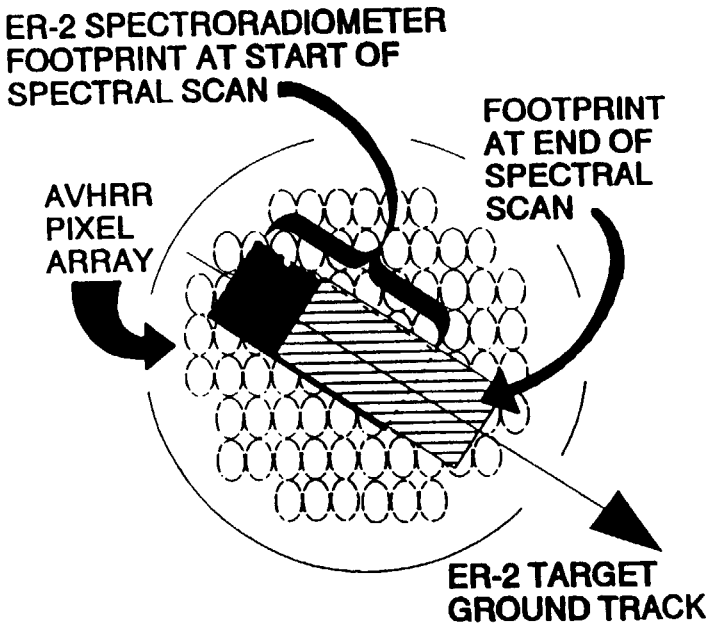

(B) SPECTRAL SAMPLING

for approximately 3 seconds in the middle of this period, and the method assumes that the two data sets correspond to identical states of scene structure and illumination.

The footprint correction is achieved by making the footprint of the aircraft spectroradiometer much larger that that of the satellite radiometer. The footprint used as the transfer standard is then the footprint of the aircraft spectroradiometer, which is well-characterized compared to that of the satellite radiometer. Initial navigational uncertainties between the aircraft and satellite pointing vectors amount to the equivalent of several footprints of the aircraft spectroradiometer. It is therefore necessary to search the satellite image to find the image displacement from nominal alignment that corresponds to maximum correlation between the set of aircraft radiance measurements and the equivalent set of counts from the satellite radiometer. This approach to fine-tuning of the navigation implies that the correct displacement is that which corresponds to the best (in a least-squares sense) linear relation between radiance and counts, and the approach is therefore unsuited to a determination of the linearity of response of the satellite radiometer. Over effectively uniform targets (such as clear ocean surface) this restriction does not apply.

The method assumes that the spectral response functions of the satellite radiometer channels have not changed since being measured before launch, and all observed changes in response in orbit are attributed to changes in gain. For NOAA-11 AVHRR the preliminary results reported here show that the gain ratio of channel 1 to channel 2 during the period November, 1988, to October, 1990, is constant to within $\pm$ 1%. This strongly suggests that neither channel has changed its spectral response during this period.

The spectroradiometer has been radiance and wavelength calibrated on an irregular schedule since the equipment was acquired for NOAA in March, 1988. The system was calibrated in a NASA/GSFC laboratory at Greenbelt, MD, before and after most flights, but the time intervals between flight and calibration usually exceeded 1 month. All calibration data were collected under ambient laboratory conditions and without the aircraft window in place. The window transmittance as a function of incidence angle was measure separately, and included in the calculations as a correction term.

Figure 3.3.3.2 illustrates the experimental arrangement in the laboratory to radiance-calibrate the 1.22 m diameter hemisphere calibration source. The spectral irradiance spectrum of a secondary standard lamp supplied by Optronic Laboratories, Inc., is transferred to an Optronic model 740A spectroradiometer equipped with a small integrating sphere at its entrance port. The purpose of the integrating sphere is to render the 740A's response to input irradiance effectively independent of the angular (and spatial) distribution of input irradiance elements at the entrance aperture of the 740A system. The (740A) irradiance to (hemisphere) radiance transfer requires accurate measurement of the diameters of the apertures in the sphere and the hemisphere, and of their separation.

The 1.22 m diameter hemisphere source is internally coated with a barium sulfate pigment embedded in a polyvinyl alcohol binder. Twelve 200W coiled-coil tungsten filament lamps are arranged internally along the great circle of the hemisphere adjacent to the flat face. Light from the lamps is baffled by a barium sulfate coated internal cylindrical section that prevents direct illumination of the exit aperture, and the flat internal face of the hemisphere is painted matt black. The lamps are independently switchable, and are run at a current of 6.500 $\pm$ 0.001 amps. Results for the uniformity, accuracy, and stability of the radiance calibration of the hemisphere have been published elsewhere [4]. Uniformity of the radiance field (with all 12 lamps lit) as a function of spatial and angular displacement from a position observing along the axis of the hemisphere was reported to be better than $\pm$0.3%.

Figure 3.3.3.2. (A) Irradiance calibration of the 740A spectrometer with an irradiance standard lamp.

(B) The irradiance calibration of the 740A spectrometer is used to radiance-calibrate the 122 cm diameter hemisphere source.

(A) IRRADIANCE CALIBRATION OF THE 740A SPECTROMETER WITH AN IRRADIANCE STANDARD LAMP.

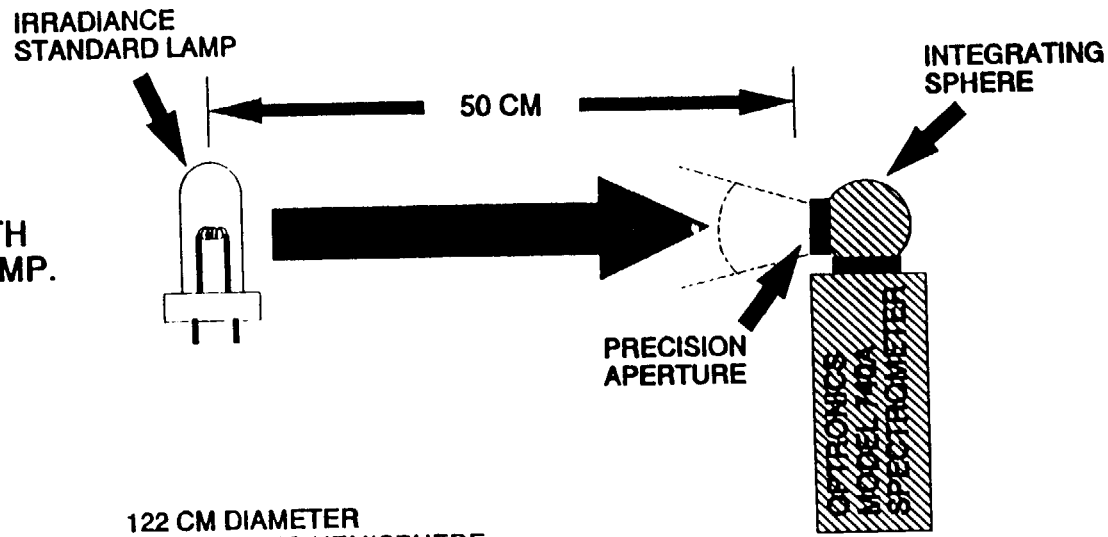

(B) THE IRRADIANCE CALIBRATION OF THE 740A SPECTROMETER IS USED TO RADIANCE-CALIBRATE THE 122 CM DIAMETER HEMISPHERE SOURCE.

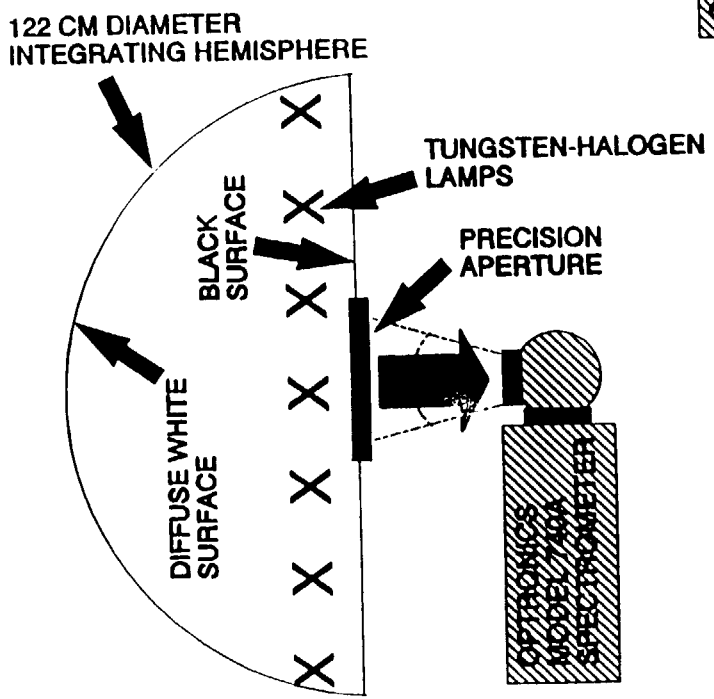

The spectroradiometer is mounted on a gimbal in the aircraft that allows its optical axis to be directed to a range of angles to the right and below the aircraft axis. These motions are controlled by an onboard minicomputer through azimuth and elevation drive motors with a positioning accuracy of approximately 1°. The optical axis passes through the center of an uncoated quartz or infrasil window (both have been used) set into the floor of the aircraft.

The silicon detector and preamplifier (EG&G HUV 4000B) is hermetically sealed behind its window. The detector responsivity near 400 nm and especially above 1000 nm is temperature dependent, so the detector temperature is actively controlled at approximately 17 C with a Peltier heat exchanger. Heating pads are wound around the body of the spectroradiometer to minimize internal temperature gradients. Under flight conditions the temperature of the supporting frame measured close to the spectroradiometer is in the range of 0 to 10 C.

The onboard minicomputer also acts to control motion of the second blocking filter and the beam blocking actuator, and supervises the recording of spectral and housekeeping data. Data are recorded with a resolution of 12 bits, and include the spectral data, frame and detector temperatures, power supply voltage, time from a dedicated clock, and gimbal azimuth and elevation. The pitch, roll, heading, and altitude of the aircraft are recorded by the separate aircraft Inertial Navigation System (INS), which has its own dedicated clock.

White Sands, NM, has been the target of choice for recent measurements, but the CZCS was successfully calibrated in 1983 by this method using clear ocean surface as the target. High reflectivity targets, such as snow and stratus cloud fields are attractive candidates for future evaluation as suitable targets.

Results

Figure 3.3.3.3 show preliminary results [5] obtained for the NOAA-11 AVHRR from 6 ER-2 flights over White Sands, NM, between November 1988 and December 1990.

The method has several major advantages: it is the only absolute method now available (excluding on-board systems), it has high intrinsic accuracy traceable to NIST standards, it requires no field work, and it can be configured for rapid response to a request for calibration information. Figure 3.3.3.3 also shows the results from Kaufman and Holben, using selected desert areas observed at annual intervals with the same observation and illumination geometry, and the results of Che et al., using White Sands to transfer the calibration of the SPOT Haute Resolution Visible (HRV) channel to AVHRR. These two methods represent, respectively, the more precise relative methods now available, and the methods for cross-calibrating sensors on the same or different platforms. The trend of gain decreasing with time shown by the aircraft results is confirmed by Che et al., and is consistent with the results of Kaufman and Holben, although the aircraft-measured absolute gain is displaced from the other results for channel 2. Figure 3.3.3b gives the results expressed as the ratio of gains for channels 1 and 2. Normalized Difference Vegetation Index (NDVI) is a function of gain ratio, which must be held constant (or measured accurately) to provide useful estimates of NDVI. The aircraft measurements indicate that the gain ratio is within $\pm$ 1%, which agrees with the results of Kaufman and Holben for the February/March periods, and disagrees with their results for August/September and with the results of Che et al.

Figure 3.3.3.3. (A) Results for the gain of NOAA-11 AVHRR as a function of time in orbit.

(B) Results for the gain ratio, which is important, for example, for the measurement of Normalized Difference Vegetation Index (NDVI).

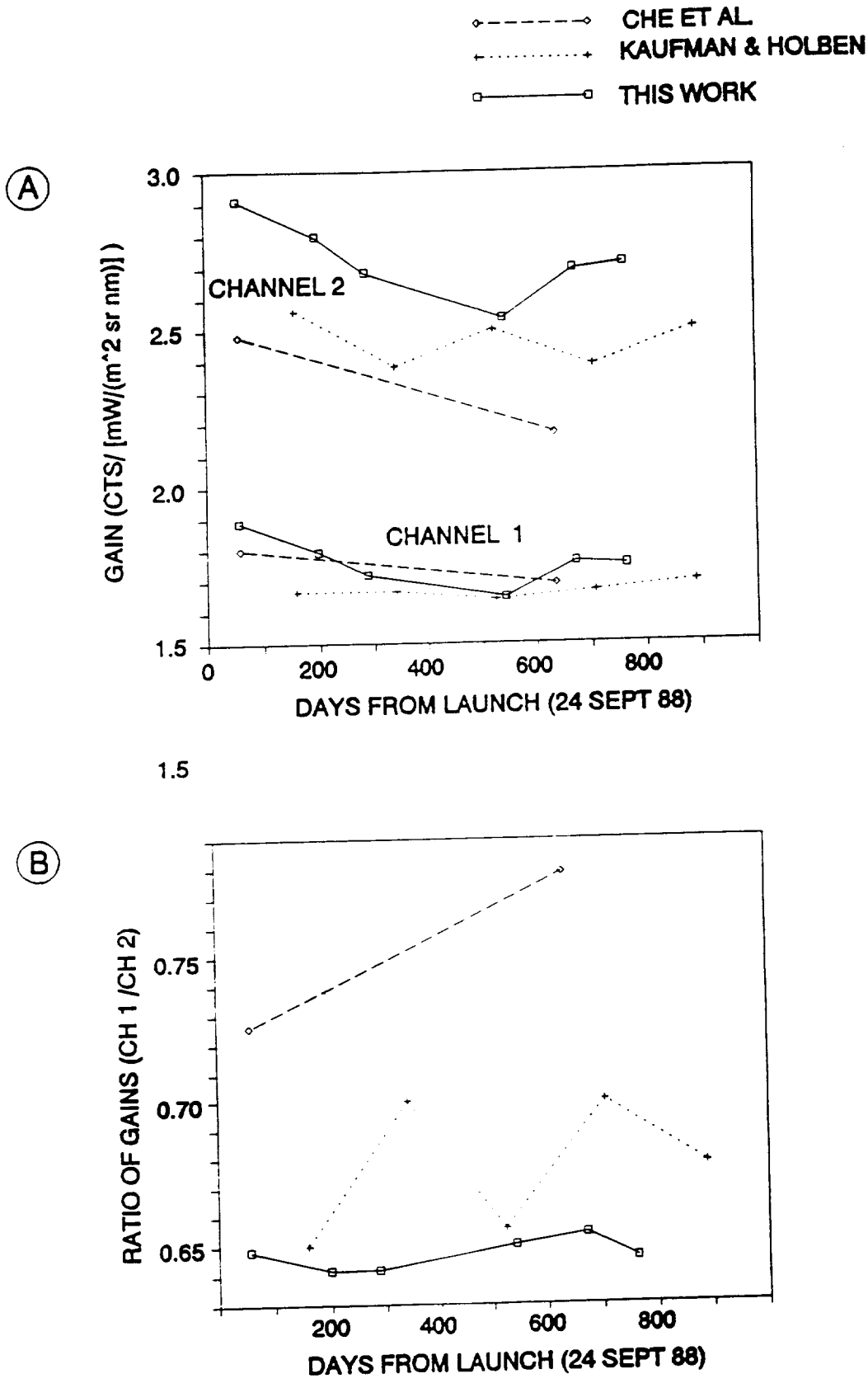
CHE ET AL.
KAUFMAN & HOLBEN
THIS WORK
A
3.0
2.5
2.0
1.5
GAIN (CTS/ [mW/(m^2 sr nm)])
CHANNEL 2
CHANNEL 1
0
200
400
600
800
DAYS FROM LAUNCH (24 SEPT 88)
1.5
B
0.75
0.70
0.65
RATIO OF GAINS (CH 1 /CH 2)
200
400
600
800
DAYS FROM LAUNCH (24 SEPT 88)

This project is now reducing data collected from the GOES-7 VISSR/VAS and from NOAA-9 AVHRR. Underflights of NOAA and GOES satellite sensors are planned for spring and fall of 1992.

References

[1] Smith, R.G., R.H. Levin, P. Abel, and H. Jacobowitz, 1988. Calibration of the solar channels of the NOAA-9 AVHRR using high altitude aircraft measurements, *J. Atmos. and Oceanic Tech.*, 5, 631-639.

[2] Hovis, W.A., J.S. Knoll, and G.R. Smith, 1985. Aircraft measurements for calibration of an orbiting spacecraft sensor, *Appl. Opts.*, 24, 407-410.

[3] Kneizys, F.X., E.P. Shettle, L.W. Abreu, J.H. Chetwynd, G.P. Anderson, W.O. Gallery, J.E.A. Selby, and S.A. Clough, 1988. Users Guide to LOWTRAN-7, Air Force Geophysics Laboratory, Environmental Paper 1010, AFGL-TR-99-0177.

[4] Guenther, B., J. McLean, and J. Cooper, 1991. Accuracy and precision actually achieved for large aperture integrating sources for aircraft and space investigations, accepted for publication in *Metrologia*.

[5] Published data:
Che, N., B.G. Grant, D.E. Flittner, P.N. Slater, and S.F. Biggar, 1991. Results of calibrations of the NOAA-11 AVHRR made by reference to calibrated SPOT imagery at White Sands, N.M., *SPIE*, 1493, 182-194.

As yet unpublished data:

Abel, P., R. Gallimore, and J. Cooper, Calibration results for NOAA-11 AVHRR channels 1 and 2 from congruent aircraft observations (in preparation).

Kaufman, Y. and B. Holben, Calibration of the AVHRR visible and near-IR bands by atmospheric scattering, ocean glint, and desert reflection (in press).

Kaufman, Y. and B. Holben, personal communication.

3.4 Target Based Calibration Methods

3.4.1 Target Related/Ground Reflectance

Phil Slater et al., University of Arizona

Approach

The reflectance of a ground target large enough to have a stable spectral reflectance over many sensor pixels is carefully measured when the image is taken by the sensor to be calibrated. At the same time, the extinction optical depth of the atmosphere is measured along with certain necessary meteorological parameters. The aerosol particle size distribution is inferred from the spectral optical depths. A radiative transfer code which accounts for multiple scattering and absorption is used to predict the in-band radiance at the entrance pupil of the sensor being calibrated. This radiance is used along with the average digital counts of the pixels corresponding to those measured on the ground to compute the calibration [1, 2]. This same method has been applied to calibrate the AVIRIS sensor in an ER-2 [3] and a Daedalus 1268 operated by EG&G in both a jet aircraft and a helicopter [4]. This method is NOT directly applicable to MODIS as the MODIS pixel size is too large for a ground crew to adequately sample the ground reflectance over multiple pixels. An modified approach, provided by the University of Arizona, is described below.

The University of Arizona group plans to make in-orbit calibrations of high spatial resolution EOS sensors such as ASTER (and HIRIS for the C platform) using a reflectance-based method described above. MODIS in-orbit calibration with reference to a ground site shall be done with a method similar to its AVHRR work [5]. The U of A group plans to continue with this type of work with future AVHRR and follow-on sensors and a MODIS simulator if it becomes available. The group plans to refine its methods to include the use of a field SWIR spectrometer, a solar radiometer designed to measure total column water vapor, and an imaging solar radiometer which will be used to study the solar aureole. The aureole is a sensitive indicator of aerosol scattering and the group hopes to improve its knowledge of the scattering phase function with this future instrument.

References

[1] Slater, P.N., S.F. Biggar, R.G. Holm, R.D. Jackson, Y. Mao, M.S. Moran, J.M. Palmer, and B. Yuan, 1987. Reflectance- and radiance-based methods for the in-flight absolute calibration of multi-spectral sensors, *Rem. Sens. of Environ.*, 22, 11-37 .

[2] Begni, G., M.C. Dinguirarad, R.D. Jackson, and P.N. Slater, 1986. Absolute Calibration of the SPOT-1 HRV Cameras, *Proc. SPIE*, Vol. 660, Earth Remote Sensing Using the Landsat Thematic Mapper and SPOT Sensor Systems, 66-76.

[3] Conel, J.E., R.O. Green, J.S. Margolis, C. Bruegge, G.A. Vane, R.E. Alley, P.N Slater, and R.D. Jackson, 1988. Field, radiometric, and spectral calibration of the airborne visible and infrared imaging spectrometer, *Proc. SPIE*, vol. 924, 179-195.

[4] Balick, L.K., C.J. Golanics, J.E. Shines, S.F. Biggar, and P.N. Slater, The in-flight calibration of a helicopter-mounted Daedalus multispectral scanner, *Proc. SPIE*, in press (1991).

[5] Teillet, P.M., P.N. Slater, Y. Mao, B. Yuan, R.J. Bartell, S.F. Biggar, R.P. Santer, R.D Jackson, and M.S. Moran, 1988. Absolute radiometric calibration of the NOAA AVHRR sensors, *Proc. SPIE*, Vol. 924, Recent Advances in Sensors, Radiometry, and Data Processing for Remote Sensing, 196-207.

3.4.2 Bio-Optical Oceans

Water leaving radiances over the many ocean locations at wavelengths greater than about 700 nm are close to zero. The satellite radiance therefore is arising entirely from the path radiance. An accurate radiative transfer model allows the path radiance to be calculated. This path radiance provides a known source which allows MODIS-N to be calibrated. The technique makes the instrument calibration and the radiative transfer model self-consistent.

Buoy measurements of pigment concentration can be compared with MODIS-N determined pigment concentrations. A discrepancy between the two may be resolved by altering the calibration of the satellite. This technique can be introduced into the routine processing and is called bio-geochemical normalization.

3.5 Image Related

3.5.1 External Image Related-Radiometric Rectification

Certain regions on Earth contain areas which are radiometrically stable. For example, exposures of bedrock may have a relatively stable reflectance over long periods of time. These radiometrically stable areas within images can be used to correct other portions of an image so that they are internally self-consistent with the stable portions of the image. The technique is generally

applied to high resolution images such as those produced by Landsat or SPOT. The applicability of the technique to MODIS-N images will be researched and applied.

3.5.2 Class-specific Scene Equalization

A generalization of the within image radiometric rectification technique in which multiple scenes are used will also be employed for monitoring the MODIS-N stability.

4 In-Orbit Geometric Calibration (?)

5 In-Orbit Spectral Calibration (Instrument Based)

6 Official MODIS-N/MCST Calibration Algorithm

6.1 Objectives/Rationale

During routine processing, one calibration algorithm will be used to determine the Level-1B radiances. This "official" algorithm may be one of the technique described above, but it is more likely to be a combination of method.

6.2 Algorithm sensitivity/simulation studies

7 Definitions and References

7.1 Data Dictionary/Glossary

7.2 Acronyms

A	
AIRS	Atmospheric Infrared Sounder
ASTER	Advanced Spaceborne Thermal Emission and Reflectance
AVHRR	Advanced Very High Resolution Radiometer
AVIRIS	Airborne Visible/Infra-Red Imaging Spectrometer
E	
EOS	Earth Observing System
EOSP	Earth Observing Scanning Polarimeter
G	
GOES	Geostationary Operational Environmental Satellite
H	
HIRIS	High Resolution Imaging Spectrometer
M	
MCST	MODIS Characterization Support Team
MERIS	Medium Resolution Imaging Spectrometer
MISR	Multi-angle Imaging Spectro-Radiometer
MODIS-N	Moderate Resolution Imaging Spectrometer - Nadir
MTF	Modulation transfer function

N

NASA	National Aeronautics and Space Administration
NOAA	National Oceanic and Atmospheric Administration

S

SeaWiFS	Sea Viewing, Wide Field-of-View Sensor
SBRC	Santa Barbara Research Center
SDSM	Solar Diffuser Stability Monitor
SRCA	Spectro-radiometric Calibration Assembly

7.3 Additional References

Flittner, D.E., and Slater, P.N., "Stability of Narrow-Band Filter Radiometers in the Solar-Reflective Range," Photogrammetric Engineering & Remote Sensing, Vol. 57, No. 2, pp. 165-171 (1991).